

## Microscopic calculation of the electron-phonon interaction in quantum wells

H. Rucker\*

*Fachbereich Physik, Humboldt Universität, Invalidenstrasse 110, D-1040 Berlin, Federal Republic of Germany*

E. Molinari

*Consiglio Nazionale delle Ricerche (CNR), Istituto "O. M. Corbino," via Cassia 1216, I-00189 Roma, Italy*

P. Lugli

*Dipartimento di Ingegneria Elettronica, II Università di Roma, I-00173 Roma, Italy*

(Received 18 June 1991)

The electron-optical-phonon scattering rates in GaAs/AlAs quantum wells are calculated on the basis of a fully microscopic description of the phonon spectra. The results indicate the great importance of confined as well as GaAs-like and AlAs-like interface phonons. By comparing our results with those of several macroscopic models, we resolve a long-standing controversy on their ability to describe the relevant vibrations.

### I. INTRODUCTION

Semiconductor superlattices (SL's) and quantum wells (QW's) have attracted increasing attention because of their improved electrical and optical properties with respect to bulk materials. The advantages offered by these layered systems (whose basic element is a heterostructure between materials with different band gaps) are essentially related to the two-dimensional (2D) confinement of electrons and holes in the narrow-band-gap material. Such a confinement is responsible for the high mobilities of the two-dimensional electron gas obtained in modulation-doped samples, as well as for the high efficiency of radiative transitions of interest in laser applications.<sup>1</sup>

Recently, several time-resolved optical techniques have been developed<sup>2</sup> that allow the study of electron and hole dynamics on a picosecond and sub-picosecond time scale. Such temporal regime, important for the study of relaxation of photoexcited carriers as well as for the incoherent tunneling across thin barriers, is dominated by the carrier interaction with the optical lattice vibrations. A coupling to acoustic phonons leads, in fact, to much slower processes.<sup>3</sup>

The layered structure of 2D systems also has profound consequences on their vibrational properties, which are strongly modified with respect to the bulk case.<sup>4</sup> Raman measurements and microscopic calculations have clearly indicated that the optical modes of GaAs/AlAs SL's and QW's are confined in either one or the other constituent; i.e., the atoms of each layer tend to vibrate at the frequency of the appropriate material. In addition, the presence of the heterointerfaces between materials with different dielectric properties leads to vibrations (the so-called macroscopic interface modes) with a potential extending into neighboring layers.<sup>4</sup>

Despite the importance of the electron-phonon interaction in determining the fast optical and electrical response of a 2D systems to external disturbances, most of the studies which have appeared in the literature either

neglect the effect of layering on the phonons, or are based on macroscopic models.<sup>5-19</sup> These models allow a great simplification in the formal treatment of the interaction, but were often obtained under rather arbitrary assumptions, particularly in the choice of boundary conditions to be imposed at the interfaces. The result has been a great proliferation of models, providing conflicting interpretations of available experimental results,<sup>20</sup> and generating much controversy and even greater confusion.

A case in point is provided by the interpretation of the experimental evidence of a relatively slow relaxation of photoexcited electrons in QW's, with characteristic cooling times that are even a factor 10 slower than the corresponding bulk results.<sup>21-24</sup> One of the solutions that has been proposed (based on the so-called "slab model,"<sup>5-7,9,12,13,16</sup>) attributes the reduced cooling to the reabsorption of nonequilibrium phonons emitted during the earlier stage of the relaxation.<sup>13,25</sup> In such a model, the electron coupling to the optical modes of the QW does not differ significantly from the coupling to bulk phonons. On the contrary, the alternative phonon description provided by the so-called "guided-mode model"<sup>8,14</sup> leads to scattering rates well below the bulk values, thus attributing the reduced cooling simply to the phonon confinement in two dimensions. Other models have also been proposed (see below).<sup>10,11,15,19</sup>

Recently<sup>26</sup> we have proposed a study of the electron-optical-phonon (*e-ph*) interaction that relies on a fully microscopic *ab initio* calculation of the phonon spectra in 2D semiconductor systems.<sup>27</sup> There, we have been able to discuss the peculiarity of such interactions without any assumptions on the boundary conditions for the vibrations, and to discriminate between the different macroscopic models. Here we will present the theoretical approach and the results in greater detail, together with a critical discussion of the different simplified schemes.

The general formal setup for the calculation is illustrated in Sec. II. In Sec. III we describe our microscopic approach, while the formulation of the macroscopic models used previously is discussed in Sec. IV. Our results for

the scattering rates are presented in Sec. V, and provide an indication for selecting the most appropriate simplified macroscopic description of vibrations at the wave vectors relevant to the interaction with carriers. In the same section we discuss the dependence of the total scattering rates on the QW thickness, and demonstrate that their value always falls between the values calculated for bulk GaAs and bulk AlAs phonons.

## II. SCATTERING RATES FOR $e$ -ph INTERACTION IN QUANTUM WELLS

In general terms, the scattering rates for the  $e$ -ph interaction are given by Fermi's "golden rule" as

$$\Gamma(u, u') = \frac{2\pi}{\hbar} |\langle u' | H | u \rangle|^2 \delta(E_{u'} - E_u), \quad (1)$$

where  $u$  and  $u'$  describe, respectively, the initial and the final states of the crystal (electrons plus phonons). For the polar interaction with phonons, the interaction Hamiltonian  $H$  is given by  $-e\varphi$ , where  $e$  is the electron charge and  $\varphi$  is the electrostatic potential associated with the lattice vibrations. In a QW, with the growth axis along the (001) direction, the total scattering rate of an electron with in-plane wave vector  $\mathbf{k}_{\parallel}$  from subband  $i$  to subband  $j$  is given by

$$\begin{aligned} \Gamma_{ij}(\mathbf{k}_{\parallel}) &= \sum_{\mathbf{k}'_{\parallel}, \nu} \Gamma_{ij}(\mathbf{k}_{\parallel}, \mathbf{k}'_{\parallel}, \nu) \\ &= \frac{2\pi e^2}{\hbar} \sum_{\mathbf{k}'_{\parallel}, \nu} |G_{ij}(\mathbf{q}_{\parallel}, \nu)|^2 (N + \frac{1}{2} \pm \frac{1}{2}) \\ &\quad \times \delta \left[ \frac{\hbar^2 \mathbf{k}_{\parallel}^2}{2m^*} - \frac{\hbar^2 \mathbf{k}'_{\parallel}{}^2}{2m^*} \mp \hbar\omega^* \right], \end{aligned} \quad (2)$$

where  $\mathbf{k}_{\parallel} = \mathbf{k}'_{\parallel} \pm \mathbf{q}_{\parallel}$ ,  $N$  is the Bose function for the phonon occupation,  $m^*$  is the electron effective mass, and the coupling factor  $G_{ij}$  is given by

$$G_{ij}(\mathbf{q}_{\parallel}, \nu) = \int \xi_i^*(z) \xi_j(z) \varphi_{\nu, \mathbf{q}_{\parallel}}(z) dz. \quad (3)$$

Here  $\xi_i(z)$  [ $\xi_j(z)$ ] is the envelope function for an electron in subband  $i$  ( $j$ ), the solution of Schrödinger's equation within the effective-mass approximation, and  $\varphi$  is the potential associated with the quantized phonon mode  $\nu$ . For a transition from subband  $i$  to subband  $j$  (often indicated as  $i \rightarrow j$ ), the term  $\hbar\omega^*$  appearing in the energy-conserving  $\delta$  function is equal to  $\hbar\omega_{\nu}(\mathbf{q}_{\parallel}) \pm (E_j - E_i)$ , which is the sum (difference) of the energy of the emitted (absorbed) optical phonon and the energy separation of the initial and final electronic subbands. For intrasubband scattering ( $i = j$ ),  $G$  is nonzero only for phonons with symmetric potentials; phonons with antisymmetric potentials contribute to the scattering between subbands of opposite parity (e.g.,  $2 \rightarrow 1$  intersubband scattering). In earlier work, most calculations assumed bulk phonons and simply neglected the effect of layering on  $\varphi$ . More recently, several proposals have been put forward in order to calculate  $\varphi$  from simple continuum approaches.<sup>5-19</sup> Such models will be examined in Sec. IV.

## III. PHONON DISPLACEMENTS AND POTENTIALS FROM THE MICROSCOPIC CALCULATION

We are interested in using an accurate microscopic lattice-dynamical approach to obtain a reliable description of the input quantities (phonon frequencies and displacements) that are needed to derive potentials and scattering rates. Following Ref. 27, the dynamical matrix  $D$  of a SL can be constructed in terms of real-space interatomic force constants derived from an *ab initio* local-density linear-response calculation performed with nonlocal norm-conserving pseudopotentials and a large plane-wave basis set. As a consequence of the very close similarity between the Ga and Al cations, the difference in the force constants of GaAs and AlAs was shown to be very small, and the force constants of the virtual crystal (i.e., of a periodic crystal with average Ga and Al pseudopotential as cationic potential) were demonstrated to reproduce the phonon spectra of bulk GaAs and AlAs and of GaAs/AlAs SL's very accurately.<sup>27</sup> We can therefore build  $D$  up by using such virtual-crystal force constants and the appropriate masses. Phonon frequencies and displacements are then obtained by direct diagonalization. The advantage of this scheme is that it has the accuracy and the predictivity of first-principles calculations, but is also tractable for systems with a large number of atoms in the unit cell, as needed here.

Before coming to a discussion of the results for dispersions and displacements, it is important to note that performing a lattice-dynamical calculation is much easier for a system with three-dimensional periodicity. We therefore simulate our GaAs QW within a supercell geometry; i.e., we extract the QW displacements from the output of a SL calculation (see below).

Figure 1 shows the phonon dispersion for a (GaAs)<sub>20</sub>/(AlAs)<sub>20</sub> (001) SL along one of the in-plane directions,  $\langle 100 \rangle$ . The angular dependence for vanishing

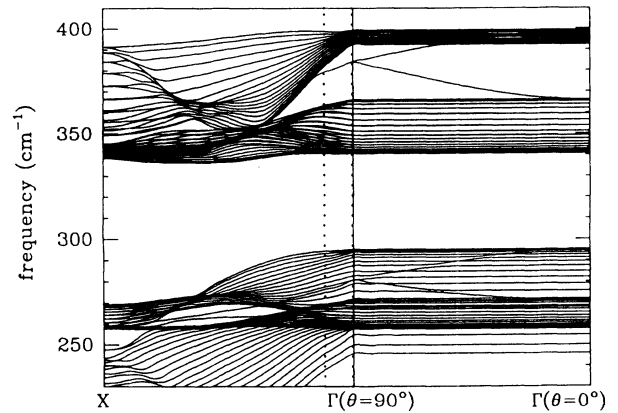


FIG. 1. Phonon dispersion of a (001)-oriented (GaAs)<sub>20</sub>/(AlAs)<sub>20</sub> SL along the in-plane (100) direction (left panel) and as a function of the  $\theta$  angle between the direction of  $\mathbf{q}$  and the growth direction at  $|\mathbf{q}| \rightarrow 0$  (right panel), calculated with the model of Ref. 27. The vertical dotted lines mark the minimum and maximum  $q_{\parallel}$ 's for an intrasubband emission process of a 0.25-eV electron (see Fig. 7).

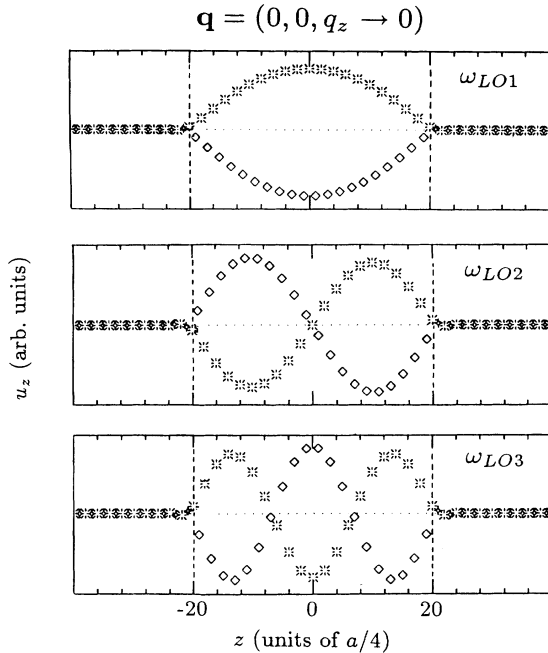


FIG. 2. Atomic displacements ( $u_z$ ) of the topmost GaAs-like modes of a (001)-oriented  $(\text{GaAs})_{20}/(\text{AlAs})_{20}$  SL for  $\mathbf{q}=(0,0,q_z \rightarrow 0)$ . The GaAs layer is centered at  $z=0$ ; the dashed vertical lines mark the As interface planes. Diamonds, stars, and asterisks indicate the positions of Ga, Al, and As planes, respectively.

wave vectors is shown in the right panel. Two separate GaAs- and AlAs-like frequency ranges can be recognized. For  $\mathbf{q} \parallel \langle 001 \rangle$ , longitudinal and transverse vibrations are decoupled. For the general directions (and in particular for  $\mathbf{q}$  parallel to the interface plane) this is no longer true. The  $z$  component of the displacements  $\mathbf{u}=(0,0,u_z)$  for

the highest GaAs-like LO modes,  $\omega_{LO1}$ ,  $\omega_{LO2}$ , and  $\omega_{LO3}$ , is shown in Fig. 2 for  $\mathbf{q}=(0,0,\varepsilon)$ , with vanishing  $\varepsilon$ . It appears that their displacements are strictly confined in GaAs and vanish in AlAs already very close to the interface. When the direction of the vanishing wave vector varies from  $\langle 001 \rangle$  ( $\vartheta=0^\circ$ ) to  $\langle 100 \rangle$  ( $\vartheta=90^\circ$ ),  $\omega_{LO1}$  shifts to a lower frequency and  $\omega_{LO2}$  becomes the highest mode. All the even-order modes,  $\omega_{LO2}, \omega_{LO4}, \dots$ , by symmetry do not shift. The sequence of the highest-frequency GaAs-like modes at  $(q_x, 0, 0)$  is shown in Fig. 3 for two different values of  $q_x$ . Indeed, by comparing Fig. 3(a) with Fig. 2, only the odd-order modes appear to be modified. Modes  $\omega_{LO2}$  and  $\omega_{LO4}$  maintain their sinelike shape. When  $q_x$  increases, all the confined modes are deformed and show a sharper decay at the interfaces. The mode originating from  $\omega_{LO1}$  shows increasing localization at interfaces with increasing  $q_{\parallel}$ , and is therefore identified as an IF mode (IF1). A second IF mode in the GaAs-like range (IF2) originates from the lowest-order confined TO mode. The same picture holds for optical modes in the AlAs-like range. In the AlAs-like range, the IF modes (Fig. 4) fall in the gap between the remaining modes of the LO and TO branches. Therefore, they show only a minor hybridization with the confined modes of the same parity.<sup>28</sup> In the GaAs-like range, instead, the IF modes and confined modes fall close in frequency, and therefore mix strongly. Previous discussions on the anisotropy of zone-center optical modes in SL's from microscopic calculations can be found in Refs. 11 and 29. It is important to notice for further considerations (see the Appendix) that also for IF modes the ions vibrate almost exclusively in one or the other material.

In polar crystals the ions have dynamical charges (Born ionic charges), producing long-range electric fields that couple to the charged carriers.<sup>30</sup> The scalar potential at position  $\mathbf{r}$  generated by the vibrating ions is

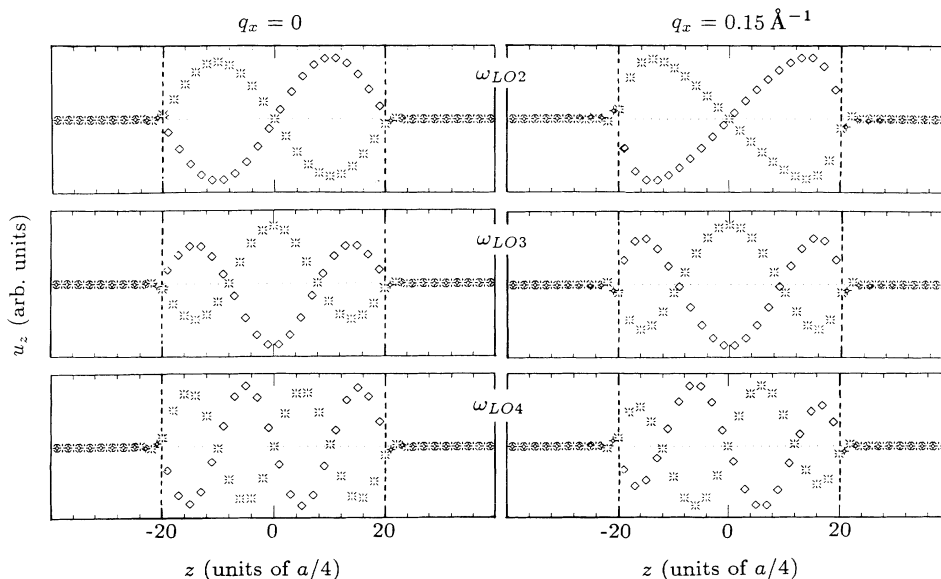


FIG. 3. Atomic displacements ( $u_z$ ) of the topmost GaAs-like modes of  $(\text{GaAs})_{20}/(\text{AlAs})_{20}$  for two different wave vectors  $\mathbf{q}=(q_x, 0, 0)$ . Notations as in Fig. 2.

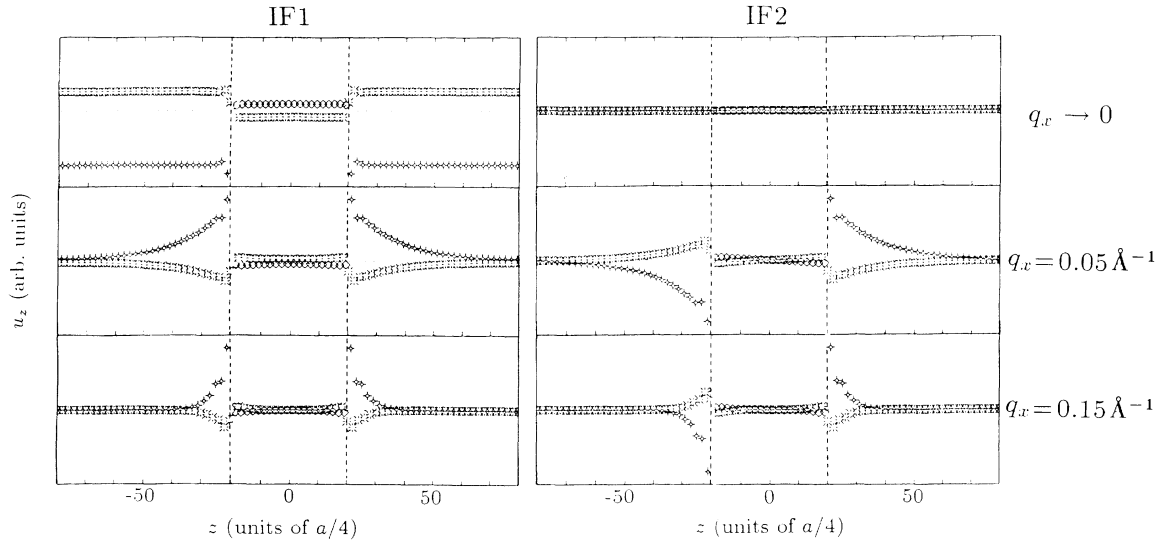


FIG. 4. Atomic displacements ( $u_z$ ) of the two AlAs-like interface modes for a  $(\text{GaAs})_{20}/(\text{AlAs})_6$  SL. Results for three different wave vectors  $\mathbf{q}=(q_x, 0, 0)$  are shown. Notations as in Fig. 2.

$$\varphi(\mathbf{r}) = - \sum_{\mathbf{R}, n} \frac{e_n^*}{4\pi\epsilon_\infty} \mathbf{u}_n(\mathbf{R}) \cdot \nabla \frac{1}{|\mathbf{r} - \mathbf{R} - \mathbf{r}_n|}, \quad (4)$$

where  $e_n^*$  is the effective charge of the  $n$ th ion located at

$\mathbf{r}_n$  in cell  $\mathbf{R}$ ;  $\epsilon_\infty$  is the high-frequency dielectric constant of the appropriate layer. The effective charges are also obtained from the first-principles calculation.<sup>27</sup> In a single QW the envelope of the potential for mode  $\mathbf{u}^v$  is given by

$$\varphi_{v\mathbf{q}_\parallel}(z) = \sum_n U^v e_n^* \left[ \frac{i\mathbf{q}_\parallel \cdot \mathbf{u}_n^v(\mathbf{q}_\parallel)}{|\mathbf{q}_\parallel|} - u_{nz}^v(\mathbf{q}_\parallel) \text{sgn}(z - z_n) \right] \times \exp(-q_\parallel |z - z_n|), \quad (5)$$

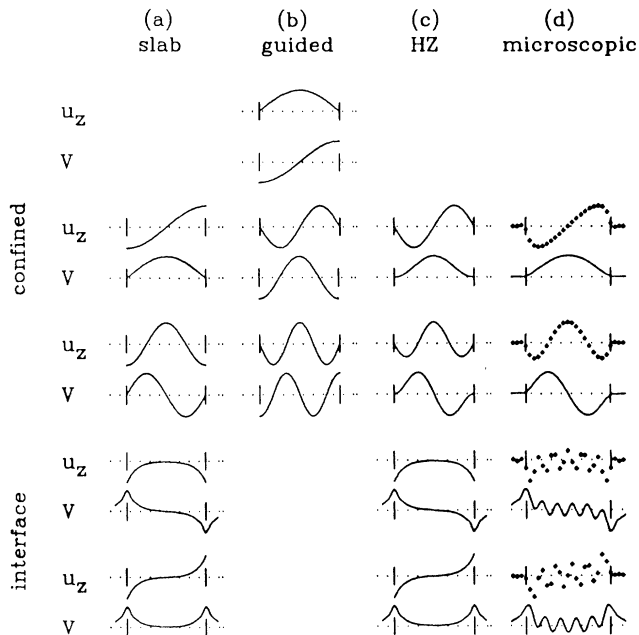


FIG. 5.  $z$  component of the atomic displacements ( $u_z$ ) and the corresponding potentials ( $V$ ) for GaAs-like optical modes in a  $(001)$ -oriented  $56\text{-}\text{\AA}$  QW surrounded by two AlAs layers. The QW interfaces are marked by vertical bars. The confined modes of highest frequency and the two interface modes are displayed from top to bottom in order of decreasing frequency. (a), (b), and (c) are from the macroscopic models; (d) shows the results of the microscopic calculation, with diamonds indicating the atomic displacements of anions. The plots are for  $q_z=0$  and  $q_\parallel=0.15\text{ \AA}^{-1}$  (one of the largest values of  $q_\parallel$  significant for the coupling).

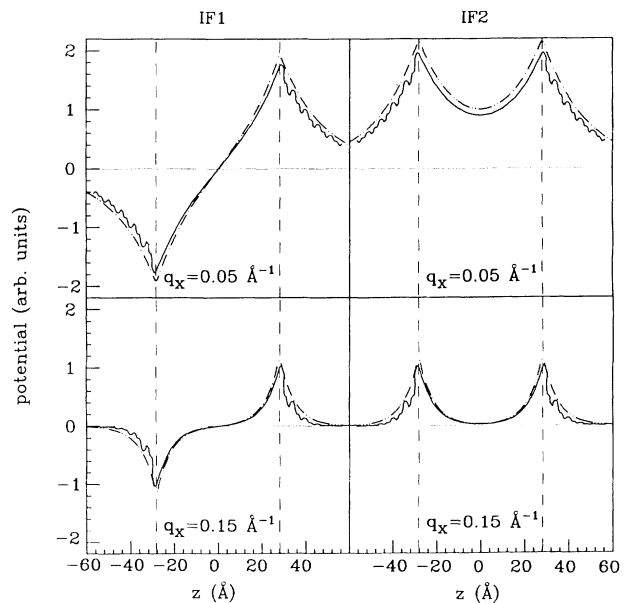


FIG. 6. Solid lines: potentials of the AlAs-like interface phonons of a  $(\text{GaAs})_{20}/(\text{AlAs})_{60}$  SL for two wave vectors  $\mathbf{q}=(q_x, 0, 0)$ . The GaAs layer is centered at  $z=0$ ; the dashed vertical lines mark the As interface planes. The dot-dashed lines are the corresponding result of dielectric continuum models.

with

$$U^v = \frac{1}{2\Omega_{\parallel}\epsilon_{\infty}} \left[ \frac{\hbar}{2N_0\omega_n(\mathbf{q}_{\parallel})} \right]^{1/2}.$$

Here  $\Omega_{\parallel}$  is the area of the 2D unit cell, and  $N_0$  is the number of lattice points in the normalization volume.

The microscopic displacements and potentials are collected in Fig. 5(d) for GaAs-like modes at  $\mathbf{q}=(0.15 \text{ \AA}^{-1}, 0, 0)$ . For AlAs-like IF modes, the potentials associated with the displacements of Fig. 4 are shown in Fig. 6 by solid lines.

#### IV. PHONON DISPLACEMENTS AND POTENTIALS FROM MACROSCOPIC MODELS

Here we will introduce and discuss the different macroscopic phonon models that have been proposed in the literature in order to clarify the reasons why they lead to drastically different results for the rate of electronic transitions in QW's and SL's. Continuum approaches for long-wavelength optical phonons are based on the equation of motion (Born Huang)<sup>30</sup>

$$\mu\ddot{\mathbf{u}}(\mathbf{r}) = -\omega_{\text{TO}}^2\mu\mathbf{u}(\mathbf{r}) + e^*\mathbf{E}(\mathbf{r}) \quad (6)$$

for the relative displacement  $\mathbf{u}$  of cations and anions, together with the following expression for the dielectric function:

$$\epsilon(\omega) = \epsilon_{\infty} \frac{\omega_{\text{LO}}^2 - \omega^2}{\omega_{\text{TO}}^2 - \omega^2}, \quad (7)$$

which connects the electric field  $\mathbf{E}$  with the electric displacement  $\mathbf{D} = \epsilon\mathbf{E}$ . Here

$$e^* = [\epsilon_{\infty}\mu\Omega(\omega_{\text{LO}}^2 - \omega_{\text{TO}}^2)]^{1/2} \quad (8)$$

is the Born effective charge and  $\mu$  is the reduced mass.  $\omega_{\text{LO}}$  and  $\omega_{\text{TO}}$  are the limiting longitudinal- and transversal-optical phonon frequencies. From (6) it follows that

$$\mathbf{E} = -\frac{e^*}{\epsilon_{\infty}\Omega}\mathbf{u} = -\nabla\varphi. \quad (9)$$

The inclusion of phonon dispersion<sup>8,15,19</sup> within hydrodynamic models, which would provide additional terms with derivatives of  $\mathbf{u}$  in the equation of motion (6), will not be discussed here.

The broken periodicity in the growth direction of a quantum-well system appears in the macroscopic model as a discontinuity of the material parameters at the interfaces. This means that the equation of motion for the quantum well may be treated by solving (6) within each medium and introducing boundary conditions at the interfaces.

The slab model,<sup>5-7,9,12,13,16</sup> which applies purely electrostatic boundary conditions at the interfaces, gives two sets of modes in the GaAs-like frequency range: (i) confined modes, whose displacements, represented by sine or cosine functions, have antinodes at the boundaries, where the potential vanishes; (ii) IF modes, whose potential and frequency strongly depend on the in-plane wave vector  $\mathbf{q}_{\parallel}$ . For large values of  $q_{\parallel}$ , the potentials are localized at the interfaces, while at small values they extend much further. The potential associated with

confined modes ( $q_z = n\pi/d$ ) has the form

$$\varphi_n(z) = C \begin{cases} \cos(q_z z), & n = 1, 3, 5, \dots \\ \sin(q_z z), & n = 2, 4, 6, \dots \end{cases} \quad (10)$$

where

$$C = \left[ \frac{\hbar(\omega_{\text{LO}}^2 - \omega_{\text{TO}}^2)}{\epsilon_{\infty}\omega_{\text{LO}}Ad} \right]^{1/2} \frac{1}{(q_z^2 + q_{\parallel}^2)^{1/2}}, \quad (11)$$

$d$  is the well thickness, and  $A$  is the in-plane normalization area. Displacements and potentials for GaAs-like modes are shown in Fig. 5(a). Clearly, the ‘‘mechanical boundary condition’’ requiring continuous displacements at the interfaces is not satisfied by this model. Nevertheless, the comparison with Fig. 3 shows that the macroscopic displacements do not differ significantly in shape from the microscopic ones for the largest  $\mathbf{q}_{\parallel}$ 's, except very close to the interfaces. The same type of agreement is reflected in the corresponding potentials (see Fig. 5). For the potentials of IF modes, see Refs. 7, 9, and 16. The plots for AlAs-like IF modes are given in Fig 6, together with a comparison with those obtained from the microscopic calculation. Note the excellent agreement between the macroscopic and microscopic results at these values of  $\mathbf{q}_{\parallel}$ , confirming the electrostatic origin of IF modes.

An alternative approach, on the contrary, imposes phonon confinement by requiring vanishing displacements at the interfaces. This implies that the electric field and potential vanish in the barrier, at least at finite  $\mathbf{q}_{\parallel}$ 's, as follows from (9). The phonon potential associated with the completely confined modes can be written as

$$\varphi_n(z) = C \begin{cases} \sin(q_z z) + \text{const}, & n = 1, 3, 5, \dots \\ \cos(q_z z) + \text{const}, & n = 2, 4, 6, \dots \end{cases} \quad (12)$$

This approach has been used by Ridley,<sup>14</sup> who assumes  $\text{const} = 0$ , i.e., potentials with antinodes at the boundaries [the ‘‘guided-mode’’ model, Fig. 5(b)]. The assumption of vanishing displacements at the interfaces rules out the existence of IF modes. The major drawback of the guided-mode model lies in its inability to fulfill electrostatic boundary conditions, accepting a discontinuity in the potential. A partial improvement can be obtained<sup>4(c)</sup> by assuming the constant in (12) to be equal to  $-1^{(n/2)+1}$  for the modes with even  $n$ , which guarantees that the potential is continuous and vanishes at the interfaces. For the modes with odd  $n$ , the continuity requirement would impose  $\text{const} = \pm 1$ , and hence a finite potential in the barrier, which in turn implies for  $\mathbf{q}_{\parallel} \neq 0$  a long-range electric force, inconsistent with the complete confinement assumed in the beginning.<sup>4(c)</sup>

Huang and Zhu (HZ) have proposed an improved macroscopic phonon model<sup>11</sup> that satisfies, besides the electrodynamic boundary conditions, the continuity of the displacements at the interface [Fig. 5(c)]. Requiring  $\varphi = 0$  and  $\partial\varphi/\partial z = 0$  at the interfaces, the scalar potential of the confined modes is

$$\varphi_n(z) = \tilde{C} \times \begin{cases} \cos(n\pi z/d) - (-1)^{n/2}, & n = 2, 4, 6, \dots \\ \sin(\mu_n\pi z/d) + C_n z/d, & n = 3, 5, 7, \dots \end{cases} \quad (13)$$

with  $\mu_3=2.86$ ,  $\mu_5=4.91$ ,  $\mu_7=6.95$ , and  $C_3=1.95$ ,  $C_5=-1.98$ ,  $C_7=2.00$ . The corresponding displacements have a vanishing  $z$  component as well as vanishing  $x, y$  components at the interfaces. The factor  $\tilde{C}$  is given by

$$\tilde{C} = \left[ \frac{\hbar(\omega_{LO}^2 - \omega_{TO}^2)}{2\epsilon_\infty \omega_{LO} A} \right]^{1/2} \times \left\{ \int_{-d/2}^{d/2} dz \left[ q_{\parallel}^2 \varphi_n^2(z) + \left( \frac{\partial \varphi_n(z)}{\partial z} \right)^2 \right] \right\}^{-1/2}. \quad (14)$$

$$\Gamma_{ij}(\mathbf{k}_{\parallel}) = \frac{e^2 m^* (\omega_{LO}^2 - \omega_{TO}^2)}{\epsilon_\infty \omega_{LO} \hbar d} (N + \frac{1}{2} \pm \frac{1}{2}) \sum_{q_z} \frac{|H_{ij}(q_z)|^2}{\left[ \left( 2k_{\parallel}^2 \mp \frac{2m^* \omega^*}{\hbar} + q_z^2 \right)^2 - 2k_{\parallel}^2 \left( k_{\parallel}^2 \mp \frac{2m^* \omega^*}{\hbar} \right) \right]^{1/2}}, \quad (15)$$

with the form factor

$$|H_{ij}(q_z)| = \int dz \zeta_i^*(z) \zeta_j(z) \times \begin{cases} \sin(q_z z) \\ \cos(q_z z) \end{cases}. \quad (16)$$

We can see that the scattering rate is now expressed as a sum over the confinement wave vector  $q_z$ . Because of the opposite symmetry of equal-order modes, the two models lead to very different scattering rates, resulting in the controversial discussion of the effect of phonon confinement on the  $e$ -ph interaction.

Part of this confusion originates from the fact that the choice of the appropriate macroscopic description to be used in the transport calculations was sometimes driven by an erroneous extrapolation of the results of Raman experiments rather than from the output of microscopic calculations that have become available in recent years.<sup>4,27,29</sup> Indeed, from off-resonance Raman spectra, generally taken in the backscattering configuration from the (001) surface, it is possible to conclude<sup>4,31</sup> that the confined mode of lowest order (and highest frequency,  $\omega_{LO1}$ ) has a nodeless displacement pattern, approximately vanishing at the interfaces; the successive modes have an increasing number of nodes and a similar behavior at interfaces. This, however, does *not* imply that such ordering applies to the wave vectors relevant for the  $e$ -ph coupling. In fact, Raman spectra in that scattering

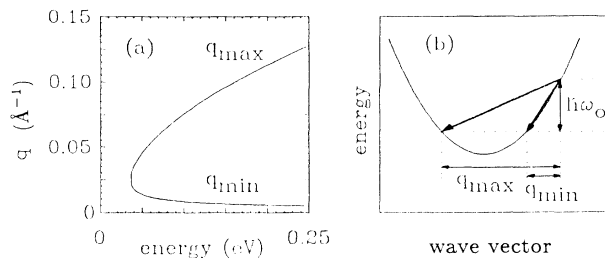


FIG. 7. (a) Minimum and maximum  $q_{\parallel}$ 's for an intrasubband emission process [sketched in (b)] vs electron energy.

In Fig. 5 the microscopic patterns of the GaAs-like modes at  $\mathbf{q}=(0.15 \text{ \AA}^{-1}, 0, 0)$  are shown together with the results of all macroscopic models discussed above. It turns out that while for small  $q_{\parallel}$ 's the best approximation is given by the HZ model, for larger  $q_{\parallel}$ 's [as the one of Fig. 5(d)] the slab model is more adequate. Indeed, the wrong boundary conditions used in this last model seem to affect only a few atomic planes close to the interfaces, where the electron wave functions of the lowest subband are small anyway (see Fig. 8 below).

Within the slab and guided models, the total scattering rate for confined modes is given explicitly by

configuration probe the lattice vibrations at  $q_{\parallel}=0$  and small values of  $q_z$ , and are indeed consistent with the microscopic results of Fig. 2. The wave vectors  $\mathbf{q}$  of interest for the treatment of  $e$ -ph scattering in QW's, instead, have the largest component *parallel* to the interfaces (the range of relevant  $q_{\parallel}$ 's is illustrated in Fig. 7), where the different ordering shown in Fig. 3 applies.

## V. SCATTERING RATES: RESULTS AND DISCUSSION

We now move to the calculation of the scattering rates for polar electron-optical-phonon interaction in a QW, based on the microscopic phonons. For the electron wave function we use the solution of Schrödinger's equations within the effective-mass approximation.<sup>3</sup> The envelope functions of subbands 1 and 2 are shown in Fig. 8.

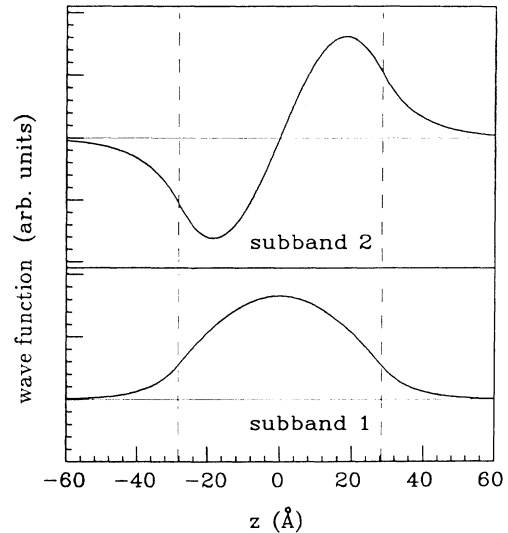


FIG. 8. Envelope function of the two lowest electronic subbands. The GaAs layer is centered at  $z=0$ ; the dashed vertical lines mark the As interface planes.

Figure 9 shows the room-temperature emission rates for the  $1 \rightarrow 1$  and  $2 \rightarrow 1$  transitions (1 and 2 indicate the two lowest subbands), obtained for a 56-Å well with a barrier height of 1 eV. We note the following: (i) The first confined mode [topmost in Fig. 5(d)] contributes to about 28% of the total  $1 \rightarrow 1$  intrasubband rate, while the third mode is already much weaker. The modes of opposite parity do not contribute. On the contrary, the second confined mode [second row in Fig. 5(d)] is the dominant one for the  $2 \rightarrow 1$  intersubband transition. (ii) The IF GaAs-like modes (shown in Fig. 9 together with the remaining confined modes because of the above-mentioned hybridization) are important, carrying about 14% of the interaction. (iii) A very strong contribution to the scattering rate comes from the AlAs-like IF modes. The importance of such modes is explained by the fact that their potential extends far into the GaAs layer at the  $q_{\parallel}$  of interest (see Fig. 6). The contribution of the remaining AlAs-like modes is negligible.

The resulting times for intrasubband and intersubband emission at room temperature are then, respectively, 0.09 and 1.0 ps, confirming that the slow cooling rate detected experimentally cannot be associated with phonon confinement, and must therefore be related to hot-phonon effects.<sup>13,25</sup> Full simulations based on our present results will be published elsewhere.<sup>32</sup>

We now compare our results for the microscopic-model phonons with those obtained, for the same struc-

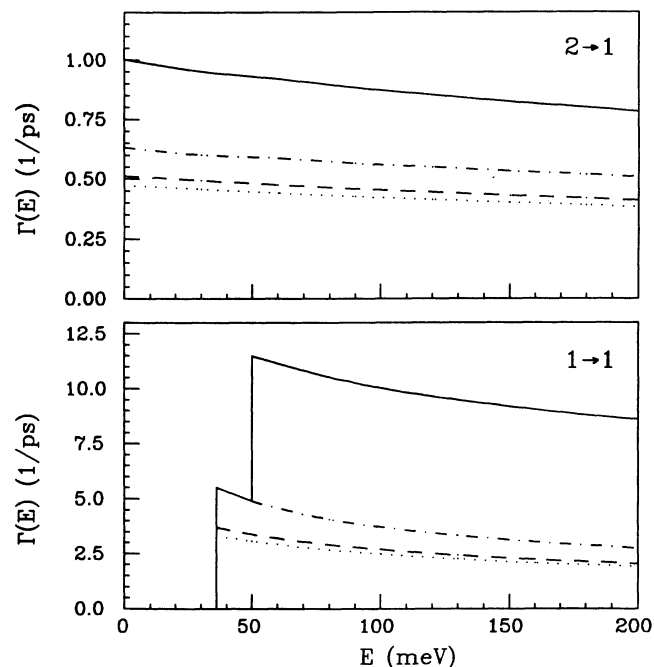


FIG. 9. Calculated total intrasubband and intersubband emission rates as a function of electron energy (solid lines), including all GaAs- and AlAs-like modes. Dashed-dotted lines show the contribution of all GaAs-like modes (including the interface ones). Dashed lines refer to the confined GaAs-like modes only, out of which the mode of lowest order (first for intrasubband and second for intersubband transitions) represents the largest contribution (dotted lines).

ture, from the models of Figs. 1(a)–1(c). In order to get comparable results from the microscopic and macroscopic calculations, we use in the macroscopic description phonon frequencies and effective charges as calculated microscopically. The parameters used are listed in Ref. 33. Figure 10 shows the contribution of GaAs-like modes to the phonon-emission rates at room temperature. The slab and HZ models (dotted and dashed lines, respectively) agree fairly well with the microscopic calculation (solid line). Such agreement can be understood from the fact that, although the microscopic displacements are not properly reproduced by the slab model at all  $q_{\parallel}$ 's, at the relevant values of  $q_{\parallel}$  their deviations are limited to a small region near the interface. The predictions of the guided-mode model are instead completely inconsistent with ours. The reason for the failure of the guided-mode model is that this model does not fulfill the electrodynamic boundary conditions at the interfaces. The total emission rates including also the interaction with AlAs-like interface modes are shown in Fig. 11. Additionally, the results for interaction of the confined electrons with bulk GaAs phonons are shown. It turns out that the use of bulk GaAs phonons is already an acceptable approximation for the total scattering rates.

All the calculations discussed so far were carried out for a 56-Å GaAs well. It should be mentioned, however, that the relative contribution of the interface modes to the total scattering depends strongly on the well thickness. Moreover, the relative contribution of GaAs- and AlAs-like IF modes changes; since the coupling of these modes to the electrons is different (much stronger in AlAs), this also produces changes in the total scattering

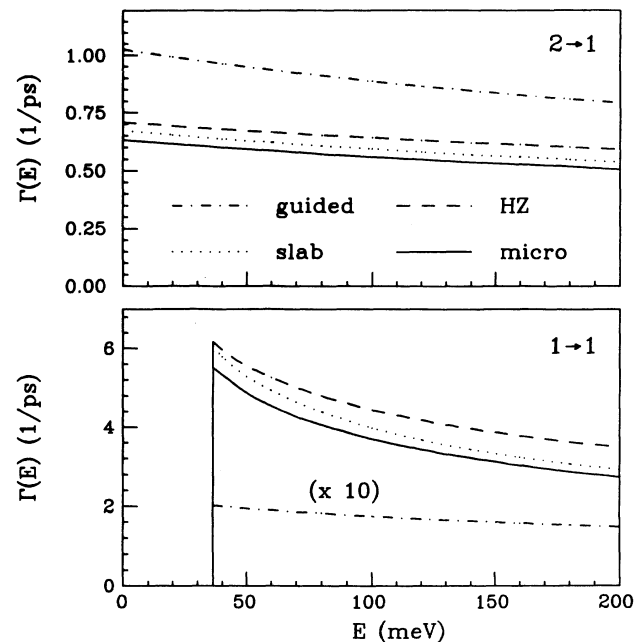


FIG. 10. Comparison of the scattering rates from our microscopic calculation with the results of macroscopic models. Only the contribution of GaAs-like modes is shown. The intrasubband rate of the guided-mode model is multiplied by a factor of 10.

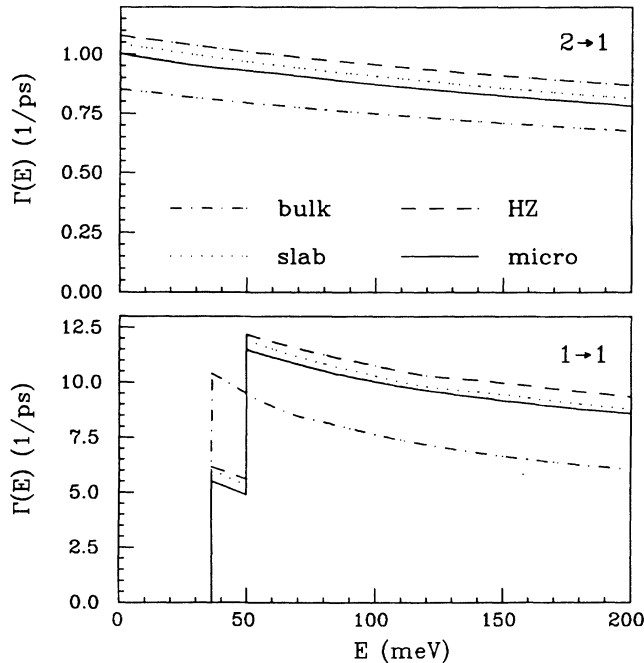


FIG. 11. Comparison of the total scattering rates (GaAs- and AlAs-like modes) from our microscopic model with the results of macroscopic models. The scattering rates for interaction with bulk GaAs phonons are also shown.

rates. The dependence of the total emission rate of a 50-meV electron in the first subband on the well thickness  $d$ , as obtained from the dielectric continuum model, is shown in Fig. 12. While for a 100-Å well this rate is well approximated by the scattering via bulk GaAs phonons, for very thin wells it tends to the AlAs phonon value. The fact that the total scattering rates always fall in the interval defined by the interaction with GaAs and with AlAs bulk phonons is true for the microscopic descrip-

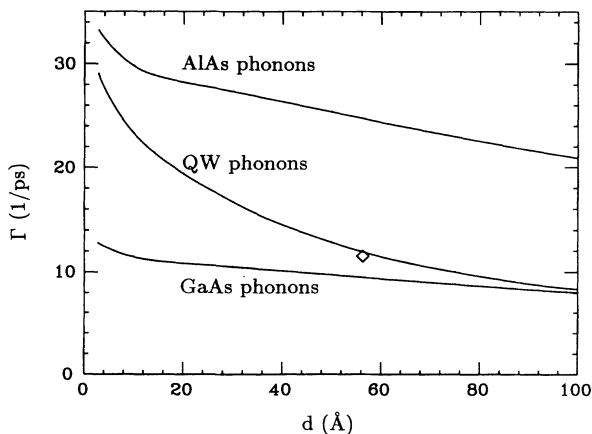


FIG. 12. Room-temperature phonon emission rate of a 50-meV electron in the first subband as a function of the well thickness. Curves for interaction with bulk GaAs and bulk AlAs phonons are shown together with the results of the dielectric continuum model (slab plus IF). The diamond indicates the result of the microscopic calculation for the 56-Å well.

tion as well, as discussed in the Appendix. The result of the microscopic calculation for the 56-Å well is included in Fig. 12 for comparison.

## VI. CONCLUSIONS

In conclusion, we have presented a calculation of the polar electron-LO-phonon interaction in GaAs/AlAs systems, based on a fully microscopic approach for the phonon spectra. The contribution of confined and GaAs- and AlAs-interface phonon modes to the electron scattering was calculated. The results indicate the importance of the interface phonon scattering, at least for wells as thin as the 56-Å well that we have considered.

While some of the macroscopic phonon models used so far lead to acceptable predictions for the scattering rates, the results of another model are completely inconsistent with the microscopic results. It turns out that the correct use of the dielectric boundary conditions is crucial for the applicability of macroscopic models to polar electron-phonon scattering.

It was demonstrated that the total scattering rates in GaAs/AlAs quantum wells fall always in between the rates given by the interaction of the confined electrons with bulk GaAs and bulk AlAs phonons. Consequently, even the rough assumption of unmodified bulk phonons may provide reasonable results. An accurate description of the phonons is instead necessary when one is interested in the contribution of individual modes, e.g., for the interpretation of the results of time-resolved spectroscopies.<sup>32</sup>

## ACKNOWLEDGMENTS

This work was supported in part by CNR, Progetto Finalizzato Calcolo Parallelo, under Grant No. 90.00658.PF69, and by IBM Corporation under agreement No. 12031053.

## APPENDIX

In this Appendix we give an estimate of the upper and lower limits for the rates of polar optical-phonon emission and absorption in QW structures. In particular, we show that in QW's the probabilities

$$\Gamma_{ij}(\mathbf{k}_{\parallel}, \mathbf{k}'_{\parallel}) = \frac{2\pi}{\hbar} \sum_{\nu} e^2 |G_{ij}(\mathbf{q}_{\parallel}, \nu)|^2 (N + \frac{1}{2} \pm \frac{1}{2}) \times \delta(E_{\mathbf{k}_{\parallel i}} - E_{\mathbf{k}'_{\parallel j}} \mp \hbar\omega_{\nu}) \quad (\text{A1})$$

of electronic transitions from state  $\mathbf{k}_{\parallel, i}$  to  $\mathbf{k}'_{\parallel, j}$  with emission (absorption) of one optical phonon always fall in between the values calculated for the interaction of the confined electrons with the bulk phonons of the two components of the QW structure.  $E_{\mathbf{k}_{\parallel i}}$  are the electronic energies. Using Eq. (3) for the coupling factor  $G_{ij}$ , we have

$$\Gamma_{ij}(\mathbf{k}_{\parallel}, \mathbf{k}'_{\parallel}) = \frac{2\pi e^2}{\hbar} (N + \frac{1}{2} \pm \frac{1}{2}) \times \int dz' \int dz \zeta_i^*(z) \zeta_j(z) \zeta_i(z') \times \zeta_j^*(z') \Phi(z, z'), \quad (\text{A2})$$

where

$$\Phi(z, z') = \sum_{\nu} \varphi_{\nu \mathbf{q}_{\parallel}}(z) \varphi_{\nu \mathbf{q}_{\parallel}}(z') \delta(E_{\mathbf{k}_{\parallel i}} - E_{\mathbf{k}_{\parallel j}} \mp \hbar \omega_{\nu}). \quad (\text{A3})$$

The sum over all phonon modes  $\nu$  in (A3) can be carried out by using the completeness relation

$$\sum_{\nu} v_{n\alpha}^*(\mathbf{q}_{\parallel}) v_{m\beta}(\mathbf{q}_{\parallel}) = \delta_{\alpha\beta} \delta_{nm}, \quad (\text{A4})$$

where  $\alpha$  and  $\beta$  indicate the Cartesian directions. The eigenvectors  $\mathbf{v}_n$  are related to the atomic displacements by  $\mathbf{v}_n = \sqrt{M_n} \mathbf{u}_n$ ,  $M_n$  being the atomic masses. As discussed in Sec. III, all the optical modes (confined and interface) of a GaAs/AlAs superlattice can be divided into a GaAs-like (opt1) and an AlAs-like (opt2) branch, and—to a good approximation—the *atomic motions* involve either the GaAs or AlAs layers. This fact allows us

to split the completeness relation (A4) into the two relations:

$$\sum_{\nu \in \text{opt1}} v_{n\alpha}^*(\mathbf{q}_{\parallel}) v_{m\beta}(\mathbf{q}_{\parallel}) + \sum_{\nu \in \text{ac}} v_{n\alpha}^*(\mathbf{q}_{\parallel}) v_{m\beta}(\mathbf{q}_{\parallel}) \times \Theta_n \Theta_m = \delta_{\alpha\beta} \delta_{nm} \Theta_n, \quad (\text{A5})$$

$$\sum_{\nu \in \text{opt2}} v_{n\alpha}^*(\mathbf{q}_{\parallel}) v_{m\beta}(\mathbf{q}_{\parallel}) + \sum_{\nu \in \text{ac}} v_{n\alpha}^*(\mathbf{q}_{\parallel}) v_{m\beta}(\mathbf{q}_{\parallel}) \times (1 - \Theta_n)(1 - \Theta_m) = \delta_{\alpha\beta} \delta_{nm} (1 - \Theta_n),$$

where  $\Theta_n = 1$  for atoms of the GaAs layers and  $\Theta_n = 0$  for the atoms of the other layer. The second sum in Eqs. (A5) contains all the acoustic modes. Using Eq. (5) for the phonon potentials and the completeness relation (A5), the coupling function  $\Phi(z, z')$  can be transformed into

$$\Phi(z, z') = \sum_n \exp(-q_{\parallel} |z - z_n|) \exp(-q_{\parallel} |z' - z_n|) [1 + \text{sgn}(z - z_n) \text{sgn}(z' - z_n)] \times [\Theta_n \gamma_n^{\text{GaAs}} \delta(E_{\mathbf{k}_{\parallel i}} - E_{\mathbf{k}_{\parallel j}} \mp \hbar \omega_{\text{LO}}^{\text{GaAs}}) + (1 - \Theta_n) \gamma_n^{\text{AlAs}} \delta(E_{\mathbf{k}_{\parallel i}} - E_{\mathbf{k}_{\parallel j}} \mp \hbar \omega_{\text{LO}}^{\text{AlAs}})], \quad (\text{A6})$$

where

$$\gamma_n = \frac{e_n^{*2} \hbar}{8 \Omega_{\parallel}^2 \epsilon_{\infty}^2 N_0 M_n \omega_{\text{LO}}}.$$

For the derivation of (A6) we have approximated the frequencies of all phonons of the GaAs- (AlAs)-like optical branches by  $\omega_{\text{LO}}^{\text{GaAs}}$  ( $\omega_{\text{LO}}^{\text{AlAs}}$ ). We have tested that the effect of this approximation on the energy-conserving  $\delta$  function is negligible for the purpose of the present demonstration. The sum over the acoustic modes appearing in (A5) was neglected, since the long-range electric fields of the acoustic modes are small compared to those of the optical modes. From (A6) one can see that the coupling function  $\Phi(z, z')$  is a sum of a part interacting with the coupling constant of GaAs and a part with the AlAs coupling. This allows us to write the transition probabilities (A1) as

$$\Gamma_{ij}(\mathbf{k}_{\parallel}, \mathbf{k}'_{\parallel}) = y \Gamma_{ij}^{\text{GaAs}}(\mathbf{k}_{\parallel}, \mathbf{k}'_{\parallel}) + (1 - y) \Gamma_{ij}^{\text{AlAs}}(\mathbf{k}_{\parallel}, \mathbf{k}'_{\parallel}), \quad (\text{A7})$$

where  $\Gamma_{ij}^{\text{GaAs}}$  and  $\Gamma_{ij}^{\text{AlAs}}$  are the rates of the considered electronic transition calculated for the interaction of the

confined electrons with bulk phonons of GaAs and AlAs, respectively. The relative weight  $y$  ( $0 \leq y \leq 1$ ) of the GaAs and AlAs branches for a given transition between electronic subbands  $i$  and  $j$  depends on the spatial region of the coupling function  $\Phi(z, z')$  that is probed by the envelope functions  $\zeta_i$  and  $\zeta_j$  of the electrons [see Eq. (A2)].

If we assume equal coupling constants for both constituents of the QW and take the macroscopic limit ( $a \rightarrow 0$ ), the coupling function (A6) transforms into the known expression for the interaction with bulk phonons:

$$\Phi(z, z') = \frac{e^{*2} \hbar}{4 \Omega A \epsilon_{\infty}^2 \mu \omega_{\text{LO}} q_{\parallel}} \exp(-q_{\parallel} |z - z'|) \times \delta(E_{\mathbf{k}_{\parallel i}} - E_{\mathbf{k}_{\parallel j}} \mp \hbar \omega_{\text{LO}}). \quad (\text{A8})$$

The fact that for equal polar electron-phonon coupling in the well and barrier materials the coupling to the phonons of the quantum well gives the same result as the coupling to unmodified bulk phonons was already shown by Ando and Mori<sup>16</sup> within the framework of the dielectric continuum model.

\*Present address: Max-Planck-Institut für Festkörperforschung, Heisenbergstr. 1, D-7000 Stuttgart 80, FRG.

<sup>1</sup>See, e.g., *Applications of Multi-Quantum Wells, Selective Doping and Superlattices*, edited by R. Dingle (Academic, New York, 1987).

<sup>2</sup>See, e.g., J. Shah, IEEE J. Quantum Electron. **QE-22**, 1728 (1986).

<sup>3</sup>S. M. Goodnick, and P. Lugli, Phys. Rev. B **37**, 2578 (1988).

<sup>4</sup>See, for example, the following reviews: (a) M. V. Klein, IEEE

J. Quantum Electron. **QE-22**, 1760 (1986); (b) B. Jusserand and M. Cardona, in *Light Scattering in Solids V*, edited by M. Cardona and G. Güntherodt, (Springer, Berlin, 1989), p. 49; (c) J. Menéndez, J. Lumin. **44**, 285 (1989); (d) A. Fasolino and E. Molinari, Surf. Sci. **228**, 112 (1990).

<sup>5</sup>F. A. Riddoch and B. K. Ridley, J. Phys. C **16**, 6971 (1983).

<sup>6</sup>E. P. Pokatilov and S. I. Beril, Phys. Status Solidi B **118**, 567 (1983).

<sup>7</sup>R. Lassnig, Phys. Rev. B **30**, 7132 (1984).

- <sup>8</sup>M. Babiker, *J. Phys. C* **19**, 683 (1986).
- <sup>9</sup>L. Wendler and R. Pechstedt, *Phys. Status Solidi B* **141**, 129 (1987).
- <sup>10</sup>C. T. Giner and F. Comas, *Phys. Rev. B* **37**, 4583 (1988).
- <sup>11</sup>K. Huang and B. Zhu, *Phys. Rev. B* **38**, 13 377 (1988).
- <sup>12</sup>R. Enderlein, F. Bechstedt, and H. Gerecke, *Phys. Status Solidi B* **148**, 173 (1988); F. Bechstedt and R. Enderlein, *ibid.* **131**, 43 (1985).
- <sup>13</sup>J. K. Jain and S. Das Sarma, *Phys. Rev. Lett.* **62**, 2305 (1989).
- <sup>14</sup>B. K. Ridley, *Phys. Rev. B* **39**, 5282 (1989).
- <sup>15</sup>T. Tsuchiya, H. Akera, and T. Ando, *Phys. Rev. B* **39**, 6025 (1989); H. Akera and T. Ando, *ibid.* **40**, 2914 (1989).
- <sup>16</sup>N. Mori and T. Ando, *Phys. Rev. B* **40**, 6175 (1989).
- <sup>17</sup>S. Rudin and T. L. Reinecke, *Phys. Rev. B* **41**, 7713 (1990); **43**, 9298(E) (1991).
- <sup>18</sup>K. W. Kim and M. A. Stroschio, *J. Appl. Phys.* **68**, 6289 (1990).
- <sup>19</sup>H. Gerecke and F. Bechstedt, *Phys. Rev. B* **43**, 7053 (1991).
- <sup>20</sup>See, for example, J. F. Ryan and H. Tatham, *Solid-State Electron.* **32**, 1429 (1989), and references cited therein.
- <sup>21</sup>J. Shah, A. Pinczuk, A. C. Gossard, and W. Wiegmann, *Phys. Rev. Lett.* **54**, 2045 (1985).
- <sup>22</sup>Z. Y. Xu and C. L. Tang, *Appl. Phys. Lett.* **44**, 692 (1984).
- <sup>23</sup>J. F. Ryan, R. A. Taylor, A. J. Turbfield, and J. M. Worlock, *Surf. Sci.* **170**, 511 (1986).
- <sup>24</sup>K. Leo, W. W. Ruhle, and K. Ploog, *Phys. Rev. B* **38**, 1947 (1988).
- <sup>25</sup>P. Lugli, P. Bordone, S. Gualdi, P. Poli, and S. M. Goodnick, *Solid-State Electron.* **32**, 1881 (1989).
- <sup>26</sup>P. Lugli, E. Molinari, and H. Rucker, *Superlatt. Microstruct.* **10**, 471 (1991); H. Rucker, E. Molinari, and P. Lugli, *Phys. Rev. B* **44**, 3463 (1991).
- <sup>27</sup>S. Baroni, P. Giannozzi, and E. Molinari, *Phys. Rev. B* **41**, 3870 (1990); E. Molinari, S. Baroni, P. Giannozzi, and S. de Gironcoli, in *Proceedings of the 20th International Conference on the Physics of Semiconductors*, edited by J. D. Joannopoulos and E. Anastassakis (World Scientific, Singapore, 1990), p. 1429; *Phys. Rev. B* **45**, 4280 (1992).
- <sup>28</sup>Note that the AlAs-like IF modes have been calculated in a (GaAs)<sub>20</sub>/(AlAs)<sub>60</sub> geometry in order to avoid the coupling of neighboring layers, at least in a wide range of  $q_{\parallel}$ 's. An even larger AlAs barrier would be necessary for the smallest  $q_{\parallel}$ 's. Fortunately, the comparison with the results of macroscopic models for IF modes (see Fig. 6) allow us to avoid the use of practically untractable supercells.
- <sup>29</sup>E. Richter and D. Strauch, *Solid State Commun.* **64**, 867 (1987); S. F. Ren, H. Chu, and Y. C. Chang, *Phys. Rev. B* **37**, 8899 (1988).
- <sup>30</sup>M. Born and K. Huang, *Dynamical Theory of Crystal Lattices* (Clarendon, Oxford, 1954).
- <sup>31</sup>A. Sood, J. Menéndez, M. Cardona, and K. Ploog, *Phys. Rev. Lett.* **54**, 2111 (1985).
- <sup>32</sup>P. Lugli, P. Bordone, E. Molinari, H. Rucker, A. M. de Paula, A. C. Maciel, J. F. Ryan, and C. T. Foxon, *Semicond. Sci. Technol.* (to be published).
- <sup>33</sup>For GaAs,  $\epsilon_{\infty} = 10.92\epsilon_0$ ,  $\hbar\omega_{LO} = 36.1$  meV,  $\hbar\omega_{TO} = 33.5$  meV,  $e^* = 2.07e$ . For AlAs,  $\epsilon_{\infty} = 8.16\epsilon_0$ ,  $\hbar\omega_{LO} = 49.6$  meV,  $\hbar\omega_{TO} = 44.5$  meV,  $e^* = 2.17e$ .